Implementation of Robust Multi-objective Optimization in the Build Orientation Problem

Marina A. Matos[1], Ana Maria A. C. Rocha[1(✉)], Lino A. Costa[1], and Ana I. Pereira[2]

[1] ALGORITMI Center, University of Minho, 4710-057 Braga, Portugal
mmatos@algoritmi.uminho.pt, {arocha,lac}@dps.uminho.pt
[2] Research Centre in Digitalization and Intelligent Robotics (CeDRI), Instituto Politécnico de Bragança, 5300-253 Bragança, Portugal
apereira@ipb.pt

Abstract. Additive manufacturing (AM) is an emerging technology to create 3D objects layer-by-layer directly from a 3D CAD model. The build orientation is a critical issue in AM and its optimization will significantly reduce the building costs and improve object accuracy. This paper aims to optimize the build orientation problem of a 3D CAD model using a robust multi-objective approach, taking into account the staircase effect and the support area characteristics. Thus, the main objective is to obtain a robust Pareto optimal front, composed of solutions that are not quite sensitive to perturbations in the variables. In this manner, a set of robust solutions is presented as alternatives and the decision-maker can identify the compromise solutions and choose according to his/her preferences.

Keywords: Additive manufacturing · 3D Printing · Robust multi-objective optimization · Build orientation

1 Introduction

3D printing is an additive manufacturing (AM) technique used by several companies for manufacturing a wide range of 3D objects. A 3D object is built from 3D model data, by adding layer-by-layer of material, using a variety of materials, such as plastic, resin, rubber, ceramics, glass, concrete and metal [1]. Currently, AM processes are being used in different areas such as medical sciences (e.g. dental restorations and medical implants), jewellery, footwear industry, automotive industry, aircraft industry among others [2–4].

This work has been developed under the FIBR3D project - Hybrid processes based on additive manufacturing of composites with long or short fibers reinforced thermoplastic matrix (POCI-01-0145-FEDER-016414), supported by the Lisbon Regional Operational Programme 2020, under the PORTUGAL 2020 Partnership Agreement, through the European Regional Development Fund (ERDF). This work has been supported by FCT – Fundação para a Ciência e Tecnologia within the R&D Units Project Scope: UIDB/00319/2020.

© Springer Nature Switzerland AG 2021
O. Gervasi et al. (Eds.): ICCSA 2021, LNCS 12953, pp. 247–259, 2021.
https://doi.org/10.1007/978-3-030-86976-2_17

In the last years, AM has been used much more efficiently to improve part quality, process planning and post-processing, while reducing processing time and cost [4]. This technology also has the advantage of better resource efficiency, the parts produced have greater durability and it is possible to produce parts on a small scale sizes and complex geometry [3]. In addition, AM has the main advantage of being flexible and allowing the development of parts produced in different orientations. Furthermore, for a given build orientation it can generate less waste of material in the production of parts and requires less time and costs in its development [3]. The selection of the best build orientation is a critical issue because it affects several factors such as the number of generated supports, printing time, material cost, final part quality, shrinkage, distortion, support volume, and support area [4,5].

In the literature, a number of studies have been carried out in order to select the optimal build orientation for a 3D CAD model. Over the years, different approaches have been taken to determine the orientation of a 3D model based on single-objective optimization [6–9]. Matos et al. in [5] used a global optimization method, the Electromagnetism-like algorithm, to optimize six printing quality measures in order to find the optimal build orientations of six 3D CAD models. Moreover, different multi-objective approaches have been developed in order to determine a set of trade-off optimal build orientations, when optimizing more than one quality measure simultaneously [10–15]. For example, in [16] the authors applied the NSGA-II multi-objective method to determine the Pareto optimal set of build orientations based on four quality measures (the support area, the build time, the surface roughness, and the overall quality of the surface).

Recently, the main focus on some multi-objective optimization studies is finding the global best solutions that are less sensitive to the perturbation of the decision variables in its neighborhood [17,18]. In this case, researchers are interested in finding the so-called robust solutions. Robust optimization aims to find robust solutions, which are solutions that are not quite sensitive to small perturbations in the variables [17]. The robust optimization deals with uncertainties in variables making the objective functions have stochastic behaviors [18].

In robust optimization, the parameters of an optimization problem are not deterministic but uncertain, since their values depend on the scenarios which may occur [19]. Over the past few years, researchers have studied the single-objective uncertain optimization problems as well as the robustness concepts for multi-objective optimization problems, where in the first case, the problems are transformed into deterministic multi-objective problems by treating each scenario as an objective function [19,20].

In this paper an implementation of robust multi-objective optimization in the build orientation problem is presented. Firstly, the robust multi-objective problem is presented in the context of the build orientation optimization of a 3D CAD model. In this study, the Rear Panel Fixed model is used. The multi-objective genetic algorithm based on NSGA-II is applied to determine the robust Pareto optimal solutions that optimize the final quality of a 3D object, based on two specific criteria: the staircase effect and the area spent with external

supports. Therefore, a step-by-step implementation of the robust multi-objective optimization for a given solution of the build orientation problem is described. Finally, the robust Pareto optimal solutions obtained are analyzed, in order to demonstrate their sensitivity towards two kinds of small perturbations in their decision variable values.

This article is organized as follows. Section 2 describes the model and the quality measures optimized in this study are presented in Sect. 3. The robust multi-objective approach is described in Sect. 4. The robustness analysis of the build orientation optimal solutions obtained in the numerical experiments is presented and discussed in Sect. 5. Finally, Sect. 6 contains the conclusions of this study.

2 Model

The 3D CAD model that will be used in this study is the Rear Panel Fixed (see Fig. 1(a)) which has vents on both sides. The size of the model is different from the side panels, but the side panels for left and right are equal [21].

Initially, the 3D model data is based on a 3D mesh model, created by structures built in CAD software and then converted into a surface tessellation language (STL) format, which is the standard file type used by the most common 3D print file formats. The STL file describes only the surface geometry of a 3D object, without color, texture, or other common attributes of the CAD model, representing the 3D solid object through triangular faces. The more complex the models are, the greater their number of triangular faces (see Fig. 1(b)).

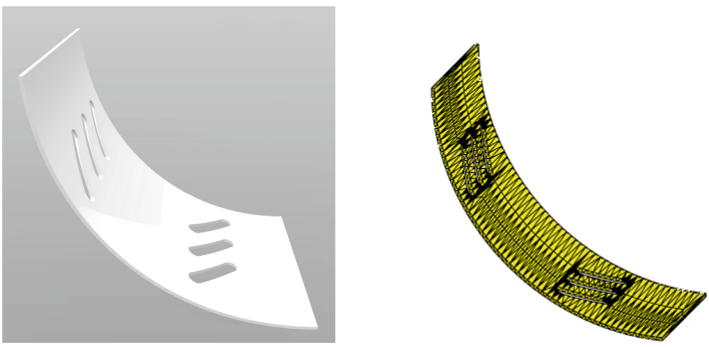

(a) 3D CAD representation

(b) Triangular representation

Fig. 1. Rear panel fixed model.

The Rear Panel Fixed model is defined by 3008 triangles, a volume of 46.2 cm^3 and 676 slices for a layer thickness of 0.2 mm (layer thickness used in this work).

3 Quality Measures

The best build orientation for a given 3D object is determined using different measures that are studied in order to obtain an improvement in the surface quality. The surface quality of an object can be influenced by many different parameters, in particular the layer thickness as well as the amount of generated supports. In this study, the build orientation optimization of a 3D model is based on two measures: the staircase effect and the support area.

The staircase effect occurs when the layers stay inside or outside the contours of the original models, giving the perception of a layer. The error associated with the staircase effect is due to the layer thickness and the slope of the part surface [6,9].

Mathematically, the staircase effect, SE, is as follows

$$SE(\theta) = \sum_i L(\theta_i) \tag{1}$$

where θ_i is the angle between triangle facet i of model surface considering the build orientation θ [5,22]. The function $L(\theta_i)$ represents the length of the step for each triangle i and it is defined by

$$L(\theta_i) = \begin{cases} \dfrac{t}{\tan(\theta_i)}, & \text{if } \tan(\theta_i) \neq 0 \\ 0, & \text{if } \tan(\theta_i) = 0 \end{cases} \tag{2}$$

where t is the layer thickness.

The other measure of the quality used in this study is called the support area, that corresponds to the total contact area of the external supports with the object [5,8,13]. Mathematically, the support area, SA, is given by

$$SA(\theta) = \sum_i A_i \left| d^T n_i \right| \gamma \tag{3}$$

where A_i is the area of the triangular facet i, d is the unit vector of the direction of construction, n_i is the normal unit vector of the triangular face i and γ is a threshold function that takes the value of 1 if $d^T n_i < 0$ and 0 if $d^T n_i > 0$ (for more details see [22]). In this study, a 3D printer with a fixed platform (z-axis) is considered so that the direction vector is $d = (0, 0, 1)$.

Figure 2 shows the SE and SA landscapes for the Rear Panel Fixed model, respectively. Note that both objective functions are nonconvex and have multiple local optima.

4 Robust Multi-objective Approach

This section presents the robust multi-objective problem approach considering the two objective functions: staircase effect and the contact supports area. An illustrative example is also presented.

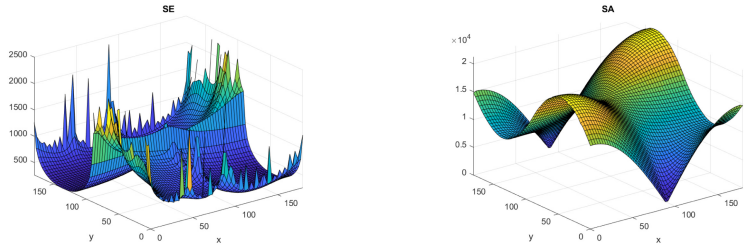

(a) Landscape of SE function (b) Landscape of SA function

Fig. 2. Landscape of SE and SA functions for the Rear Panel fixed model.

4.1 Robust Multi-objective Problem

In this study, a robust multi-objective problem, with respect to δ-neighborhood, is defined by

$$\begin{aligned} &\min \left\{ f_1^{\text{eff}}(\theta), f_2^{\text{eff}}(\theta) \right\} \\ &\text{s.t.} \quad \theta \in S \end{aligned} \tag{4}$$

where $\theta = (\theta_x, \theta_y)$ is the decision variables vector, $S = [0, 180]^2$ is the feasible search space and f_j^{eff}, for $j = 1, 2$, is a mean effective objective function given by

$$f_j^{\text{eff}}(\theta) = \frac{1}{|B_\delta(\theta)|} \int_{\alpha \in B_\delta(\theta)} f_j(\alpha) d\alpha \tag{5}$$

where the set $B_\delta(\theta) = \{(\alpha_x, \alpha_y) \in \mathbb{R}^2 : \theta_x - \delta \leq \alpha_x \leq \theta_x + \delta,\ \theta_y - \delta \leq \alpha_y \leq \theta_y + \delta\}$ is the δ-neighborhood of the solution θ and $|B_\delta(\theta)|$ is the hypervolume of the chosen δ-neighborhood.

Given a point θ, to compute the mean effective objective function, $f_j^{\text{eff}}(\theta)$ defined in (5), for $j = 1, 2$, for a given perturbation of δ, the simple bounds θ^l and θ^u should be calculated as follows. The lower bound should be determined as $\theta^l = \max(0, \theta - \delta \mathbf{1})$ and the upper bound is defined as $\theta^u = \min(\theta + \delta \mathbf{1}, 180)$, considering the lower and upper bounds of the set S and $\mathbf{1}$ representing the vector with the same dimension as θ with ones in all coordinates.

Since the set $B_\delta(\theta)$ is a rectangular region, the hypervolume can be calculated as $|B_\delta(\theta))| = (\theta_x^u - \theta_x^l)(\theta_y^u - \theta_y^l)$.

The function $f_1^{\text{eff}}(\theta)$ represents the mean effective objective function associated with the staircase effect (SE) and can be calculated as

$$f_1^{\text{eff}}(\theta) = SE^{\text{eff}}(\theta) = \frac{1}{|B_\delta(\theta)|} \int_{\theta_y^l}^{\theta_y^u} \int_{\theta_x^l}^{\theta_x^u} SE(\alpha_x, \alpha_y) d\alpha_x d\alpha_y \tag{6}$$

where $SE(\theta)$ was defined in (1).

Similarly, the function $f_2^{\text{eff}}(\theta)$ represents the mean effective objective function associated with the support area (SA) and can be calculated as

$$f_2^{\text{eff}}(\theta) = SA^{\text{eff}}(\theta) = \frac{1}{|B_\delta(\theta)|} \int_{\theta_y^l}^{\theta_y^u} \int_{\theta_x^l}^{\theta_x^u} SA(\alpha_x, \alpha_y) d\alpha_x d\alpha_y \tag{7}$$

where $SA(\theta)$ was defined in (3).

To solve the double integrals Simpson or Trapezoidal rules can be applied.

4.2 Illustrative Example

To illustrate the calculation of the mean effective objective functions, the orientation point $\theta = (90, 0)$ and the perturbation $\delta = 2$ were considered.

In this case, the set $B_2(90, 0)$ is defined as

$$B_2(90, 0) = \{(\alpha_x, \alpha_y) \in \mathbb{R}^2 : 88 \leq \alpha_x \leq 92,\ 0 \leq \alpha_y \leq 2\}$$

and the hypervolume is $|B_2(90, 0)| = 4 \times 2 = 8$.

The next step is to calculate the double integral defined in (6) and (7). In this case, the trapezoidal rule with $n = 4$ subintervals was used, having stepsizes of $h_x = 1$ and $h_y = 0.5$ associated to the variables α_x and α_y, respectively. Then, the domain region $B_2(90, 0)$ will be discretized as shown in Table 1.

Table 1. Discretized values of α_x and α_y for $n = 4$ subintervals.

j	0	1	2	3	4
α_x^j	88.0	89.0	90.0	91.0	92.0
α_y^j	0.0	0.5	1.0	1.5	2.0

In order to compute the double integral, the values of $SE(\alpha_x^i, \alpha_y^j)$, $i, j = 0, \ldots, 4$ are presented on Table 2.

Table 2. $SE(\alpha_x^i, \alpha_y^j)$ values for $i, j = 1, \ldots, 4$.

$SE(\alpha_x^i, \alpha_y^j)$	α_x^0	α_x^1	α_x^2	α_x^3	α_x^4
α_y^0	1917.3	3346.3	31705.7	4517.6	2393.5
α_y^1	1870.2	3038.4	6243.0	3143.4	1982.8
α_y^2	1753.1	2497.0	3351.8	2536.8	1785.3
α_y^3	1609.5	2058.4	2390.0	2072.7	1615.5
α_y^4	1470.5	1753.6	1918.6	1756.1	1465.6

Considering the auxiliar function, $\overline{SE}(\alpha_y^j)$, $j = 0, \ldots, 4$,

$$\overline{SE}(\alpha_y^j) \approx \frac{h_x}{2} \left[SE(\alpha_x^0, \alpha_y^j) + 2 \sum_{i=1}^{n-1} SE(\alpha_x^i, \alpha_y^j) + SE(\alpha_x^n, \alpha_y^j) \right],$$

Table 3. $\overline{SE}(\alpha_y^j)$values.

j	0	1	2	3	4
$\overline{SE}(\alpha_y^j)$	41725.0	14351.0	10155.0	8133.5	6896.3

where the calculated values of $\overline{SE}(\alpha_y^j)$, $j = 0, \ldots, 4$, are shown in Table 3.

Finally, the approximation of the double integral is given by

$$SE^{\text{eff}}(90, 0) \approx \frac{1}{8}\frac{h_y}{2}\left[\overline{SE}(\alpha_y^0) + 2\sum_{j=1}^{n-1}\overline{SE}(\alpha_y^j) + \overline{SE}(\alpha_y^n)\right] = \frac{28475.0}{8} = 3559.4.$$

In a similar way, the value of $SA^{\text{eff}}(90, 0)$ is obtained as,

$$SA^{\text{eff}}(90, 0) = \frac{9935.2}{8} = 1241.9.$$

5 Experiments

The numerical results are presented in this section.

5.1 Details

In this paper, the elitist NSGA-II proposed by Deb et al. [23] implemented in the `gamultiobj` function from MATLAB® [24] environment is used to solve the bi-objective robust optimization problem defined in (4), where SE^{eff} is given by (6) and SA^{eff} is given by (7). More information on the topics mentioned above can be found in [21].

The population size and the maximum number of generations was set to 50 (default value) and 600, respectively. The default values for the remaining parameters of the `gamultiobj` function were used. Due to the stochastic nature of the optimization algorithm, 30 independent runs were performed. By default, the Pareto fraction is 0.35 and therefore, in each run, 18 non-dominated solutions are found (0.35 × population size). The *Simplify 3D* software (a 3D model printing simulator) allows to visualize the solutions found for the Rear Panel fixed model [25].

5.2 Results

In this section, the results obtained for the Rear Panel Fixed for two different values of δ-neighborhood are discussed. The approximations to the robust Pareto optimal fronts for the robust bi-objective optimization problem for $\delta = 1$ and $\delta = 2$ are presented.

In the following graphs, the set of robust non-dominated solutions obtained among the 30 independent runs are plotted with a red circle. Representative

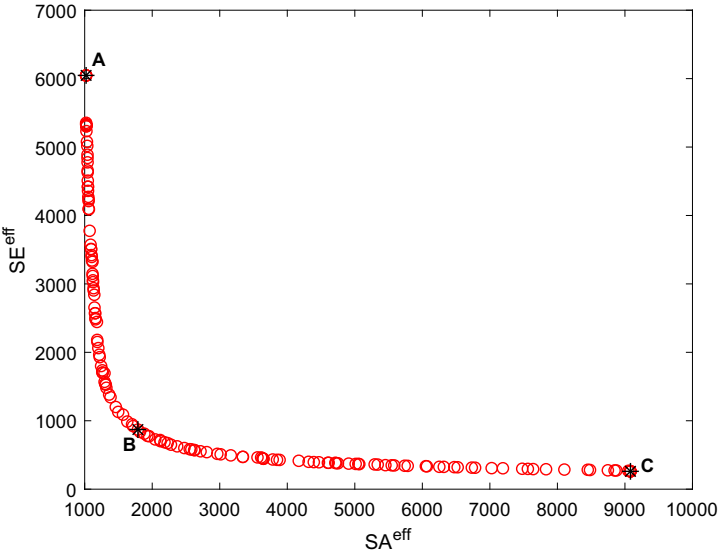

Fig. 3. Robust Pareto front obtained for SA vs. SE problem with $\delta = 1$. (Color figure online)

efficient solutions (marked with a black asterisk) are selected from the robust Pareto fronts and considered to analyze the trade-offs between the objectives and identify the characteristics associated to these solutions.

Figure 3 shows the robust Pareto front obtained for SA^{eff} vs. SE^{eff} problem with $\delta = 1$. It can be seen that solution A is the solution with the best value of SA^{eff} and solution C is the solution with best value of SE^{eff}. On the other hand, solution B is near the elbow curvature of the robust Pareto front. This solution seems to be a good trade-off since a small improvement in SA^{eff} will cause a large deterioration in SE^{eff}.

In Table 4, for the selected solutions from the robust Pareto front, the decision variable values, θ_x and θ_y, and the corresponding SA^{eff} and SE^{eff} values for $\delta = 1$ are presented.

Table 4. Robust solutions for $\delta = 1$ perturbation.

	θ_x	θ_y	SA^{eff}	SE^{eff}
A	90.45	0.00	1021.19	6047.18
B	93.66	4.66	1788.09	871.43
C	180.00	44.95	9081.89	260.74

It can be observed that solution A with the best SA^{eff} value corresponds to $\theta_x = 90.45$ and $\theta_y = 0.00$. It should be noted that, for instance, solution

$\theta_x = 90.00$ and $\theta_y = 0.00$ does not belong to the robust Pareto-optimal set for $\delta = 1$, i.e., it is not robust for a perturbation level of $\delta = 1$. This solution was found as a non-dominated solution without considering robustness in [21].

Solution C with $\theta_x = 180$ and $\theta_y = 44.95$ has the best value of SE^{eff}. Note that this solution is also obtained without considering robustness (see [21]) and, therefore, it is a robust solution.

Solution B with $\theta_x = 93.66$ and $\theta_y = 4.66$ may be interesting for the decision-maker since moving to neighbor solutions is not attractive in terms of the trade-offs between SA^{eff} and SE^{eff}.

In Fig. 4, the robust Pareto front obtained for SA^{eff} vs. SE^{eff} problem with $\delta = 2$ is presented.

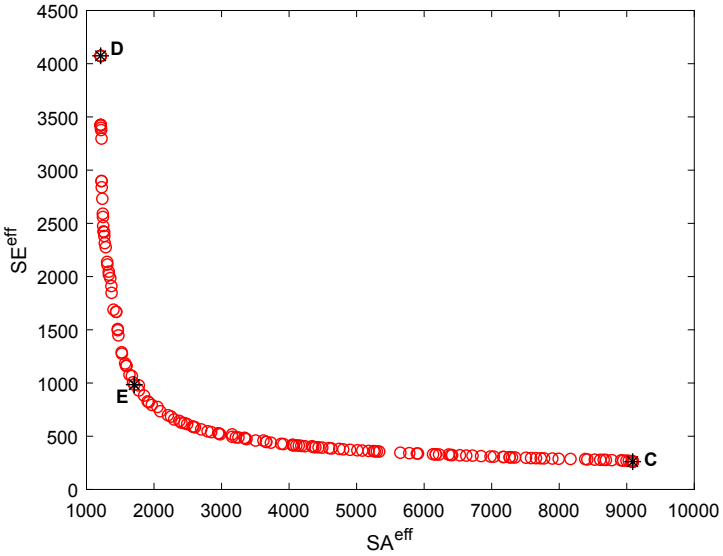

Fig. 4. Robust Pareto front obtained for SA vs. SE problem with $\delta = 2$

Solutions in this robust Pareto front are different in terms of SE^{eff} values when compared with those of Fig. 3. In this figure, solution D has the best SA^{eff}. Conversely, solution C has the best value of SE^{eff}. Solution E is a trade-off solution between the two objectives.

When the robust Pareto fronts from Fig. 3 and Fig. 4 with different values of δ are compared, it can be seen that the minimum SA^{eff} portion of the Pareto fronts becomes more and more non-robust. It can be observed a movement of the robust Pareto front along the complete range of optimal solutions due to the average function values computed by Eq. (5). In the minimum SE^{eff} portion of the Pareto fronts, the solutions are more robust since this effect is not observed. Actually, the extreme solution C is the same in both robust Pareto fronts. Thus, the minimum SA^{eff} region is more sensitive to decision variables perturbations

than the minimum SE^{eff} region, for which the two robust Pareto fronts are almost identical. In terms of decision variables, it can be seen that fluctuations or perturbations in θ_x represents a great effect is SE^{eff} values.

Table 5. Robust solutions for $\delta = 2$ perturbation.

	θ_x	θ_y	SA^{eff}	SE^{eff}
D	90.95	0.00	1209.47	4074.10
E	93.47	3.75	1707.54	984.67
C	180.00	44.95	9081.89	260.74

Table 5 shows the decision variables and SA^{eff} and SE^{eff} for selected solutions from the robust Pareto front for $\delta = 2$. It can be observed that solution D with the best SA^{eff} value corresponds to $\theta_x = 90.95$ and $\theta_y = 0.00$. This extreme solution D is different from the solution A obtained with $\delta = 1$. This means that solution A is robust for $\delta = 1$, but becomes non-robust for $\delta = 2$. As for a perturbation of $\delta = 1$, solution C with $\delta_x = 180$ and $\delta_y = 44.95$ is robust and the best in terms of SE^{eff}. Solution E with $\theta_x = 93.87$ and $\theta_y = 3.75$ is an intermediate alternative for the decision-maker in terms of SA and SE.

In Table 6 the decision variable values, and the SA and SE values computed by (3) and (1), for the selected solutions from the robust Pareto fronts for $\delta = 1$ and $\delta = 2$ are presented.

Table 6. Computed values for the robust solutions for $\delta = 1$ and $\delta = 2$. perturbation

	Optimal solutions		Values from (3) and (1)		Robustness	
	θ_x	θ_y	SA	SE	$\delta = 1$	$\delta = 2$
A	90.45	0.00	961.56	6902.95	✓	×
D	90.95	0.00	1087.50	5497.59	✓	✓
E	93.47	3.75	1628.65	957.02	✓	✓
B	93.66	4.66	1769.92	867.97	✓	✓
C	180.00	44.95	9078.06	260.39	✓	✓

In this table, it is also indicated the robustness of solutions for each value of δ. Taking into account the values of SA and SE computed by (3) and (1), it can be observed that all these solutions are non-dominated solutions. All solutions are robust to small perturbations of $\delta = 1$. However, solution A is not robust for $\delta = 2$. Moreover, it can be observed that $\theta_y = 0$ for solution D and A. The variation on the objective function values is due to the θ_x decision variable. A perturbation on θ_x produces a significant effect, specially, on SE values as can be seen in Table 6.

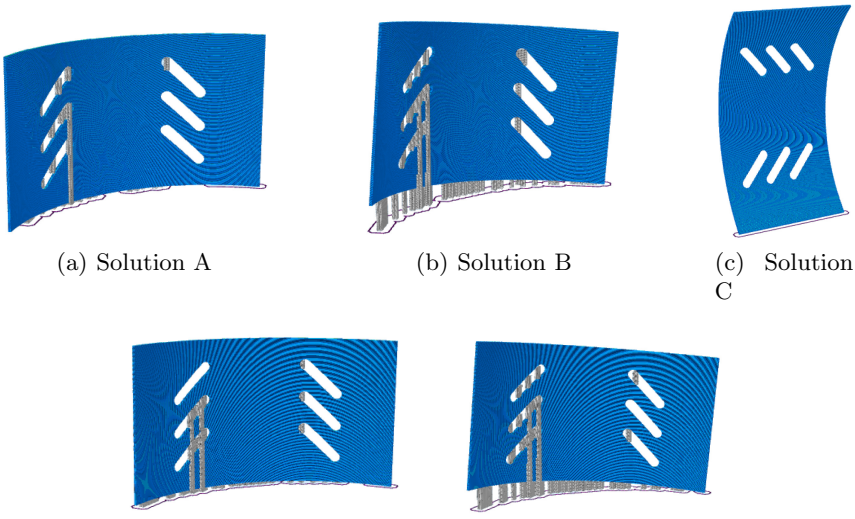

(a) Solution A (b) Solution B (c) Solution C

(d) Solution D (e) Solution E

Fig. 5. Visualization of the representative robust solutions.

In Fig. 5, the orientations of the representative robust solutions can be visualized. Solution A is not robust for $\delta = 2$ due the sensitivity of SA and SE to variations on θ_x. This can be observed in Fig. 5(a) and Fig. 5(d) where a small variation on θ_x changes the support area as well as the staircase effect. This can be seen in Fig. 2(a) in which in the vicinity of $\theta_x = 90$ and $\theta_y = 0$, there exist a large variability of the values of SE. For robust solutions D, E and B, as θ_x increases, the value θ_y also increases in a small amount. Their representations given in Fig. 5(d), Fig. 5(e) and Fig. 5(b) show the increase of support area and the reduction of the staircase effect due to the gradual change of orientation. In Fig. 2(a) and Fig. 2(b), it can be seen that from in the vicinity of $\theta_x = 90$ and $\theta_y = 0$ towards the region close to $\theta_x = 180$ and $\theta_y = 45$, there exist a plateau in both objectives and therefore, the solutions are robust. Solution C, represented in Fig. 5(c), has the largest support area due to its vertical position and the smallest staircase effect. This is a robust solution since the variability around this point is very small as can be observed in Fig. 2(a) and Fig. 2(b).

6 Conclusions

The build orientation optimization of 3D parts is one of the crucial factors to obtain the best final quality of the part surface.

In this work, an implementation of the robust multi-objective optimization in the build orientation problem was presented. Two quality measures were used in order to find robust optimal solutions for the Rear Panel Fixed model: the staircase effect and the support area.

The robust multi-objective optimization is briefly described. The experiments were conducted for two perturbation values $\delta = 1$ and $\delta = 2$.

The robust Pareto fronts obtained with the two different perturbation values, composed of solutions that were not quite sensitive to perturbations, were analyzed and compared. It was possible to conclude that small perturbations in the first component of θ represents a great effect in the SE^{eff} function.

In this way, the robust solutions will help the decision-maker to identify the compromise solutions and choose the best build orientation according to his/her preferences.

References

1. Ngo, T.D., Kashani, A., Imbalzano, G., Nguyen, K.T., Hui, D.: Additive manufacturing (3D printing): a review of materials, methods, applications and challenges. Compos. Part B Eng. **143**, 172–196 (2018)
2. Bikas, H., Stavropoulos, P., Chryssolouris, G.: Additive manufacturing methods and modelling approaches: a critical review. Int. J. Adv. Manuf. Technol. **83**(1–4), 389–405 (2016)
3. Ford, S., Despeisse, M.: Additive manufacturing and sustainability: an exploratory study of the advantages and challenges. J. Clean. Prod. **137**, 1573–1587 (2016)
4. Zhang, Y., De Backer, W., Harik, R., Bernard, A.: Build orientation determination for multi-material deposition additive manufacturing with continuous fibers. Procedia CIRP **50**(2016), 414–419 (2016)
5. Matos, M.A., Rocha, A.M.A.C., Pereira, A.I.: Improving additive manufacturing performance by build orientation optimization. Int. J. Adv. Manuf. Technol., 1–13 (2020)
6. Pereira, S., Vaz, A., Vicente, L.: On the optimal object orientation in additive manufacturing. Int. J. Adv. Manuf. Technol. **98**(5–8), 1685–1694 (2018)
7. Phatak, A.M., Pande, S.: Optimum part orientation in rapid prototyping using genetic algorithm. J. Manuf. Syst. **31**(4), 395–402 (2012)
8. Rocha, A.M.A.C., Pereira, A.I., Vaz, A.I.F.: Build orientation optimization problem in additive manufacturing. In: Gervasi, O., et al. (eds.) ICCSA 2018. LNCS, vol. 10961, pp. 669–682. Springer, Cham (2018). https://doi.org/10.1007/978-3-319-95165-2_47
9. Thrimurthulu, K., Pandey, P.M., Reddy, N.V.: Optimum part deposition orientation in fused deposition modeling. Int. J. Mach. Tools Manuf. **44**(6), 585–594 (2004)
10. Brika, S.E., Zhao, Y.F., Brochu, M., Mezzetta, J.: Multi-objective build orientation optimization for powder bed fusion by laser. J. Manuf. Sci. Eng. **139**(11), 111011 (2017)
11. Golmohammadi, A., Khodaygan, S.: A framework for multi-objective optimisation of 3D part-build orientation with a desired angular resolution in additive manufacturing processes. Virtual Phys. Prototyping **14**(1), 19–36 (2019)
12. Gurrala, P.K., Regalla, S.P.: Multi-objective optimisation of strength and volumetric shrinkage of FDM parts: a multi-objective optimization scheme is used to optimize the strength and volumetric shrinkage of FDM parts considering different process parameters. Virtual Phys. Prototyping **9**(2), 127–138 (2014)

13. Matos, M.A., Rocha, A.M.A.C., Costa, L.A., Pereira, A.I.: A multi-objective approach to solve the build orientation problem in additive manufacturing. In: Misra, S., et al. (eds.) ICCSA 2019. LNCS, vol. 11621, pp. 261–276. Springer, Cham (2019). https://doi.org/10.1007/978-3-030-24302-9_19
14. Mele, M., Campana, G.: Sustainability-driven multi-objective evolutionary orienting in additive manufacturing. Sustain. Prod. Consumption (2020)
15. Padhye, N., Deb, K.: Multi-objective optimisation and multi-criteria decision making in SLS using evolutionary approaches. Rapid Prototyping J. **17**(6), 458–478 (2011)
16. Matos, M.A., Rocha, A.M.A.C., Costa, L.A.: Many-objective optimization of build part orientation in additive manufacturing. Int. J. Adv. Manuf. Technol., 1–16 (2020)
17. Deb, K., Gupta, H.: Searching for robust pareto-optimal solutions in multi-objective optimization. In: Coello Coello, C.A., Hernández Aguirre, A., Zitzler, E. (eds.) EMO 2005. LNCS, vol. 3410, pp. 150–164. Springer, Heidelberg (2005). https://doi.org/10.1007/978-3-540-31880-4_11
18. Deb, K., Gupta, H.: Introducing robustness in multi-objective optimization. Evol. Comput. **14**(4), 463–494 (2006)
19. Botte, M., Schöbel, A.: Dominance for multi-objective robust optimization concepts. Eur. J. Oper. Res. **273**(2), 430–440 (2019)
20. Sülflow, A., Drechsler, N., Drechsler, R.: Robust multi-objective optimization in high dimensional spaces. In: Obayashi, S., Deb, K., Poloni, C., Hiroyasu, T., Murata, T. (eds.) EMO 2007. LNCS, vol. 4403, pp. 715–726. Springer, Heidelberg (2007). https://doi.org/10.1007/978-3-540-70928-2_54
21. Matos, M.A., Rocha, A.M.A.C., Costa, L.A., Pereira, A.I.: Multi-objective optimization in the build orientation of a 3D CAD model. In: Gaspar-Cunha, A., Periaux, J., Giannakoglou, K.C., Gauger, N.R., Quagliarella, D., Greiner, D. (eds.) Advances in Evolutionary and Deterministic Methods for Design, Optimization and Control in Engineering and Sciences. CMAS, vol. 55, pp. 99–114. Springer, Cham (2021). https://doi.org/10.1007/978-3-030-57422-2_7
22. Jibin, Z.: Determination of optimal build orientation based on satisfactory degree theory for RPT. In: Ninth International Conference on Computer Aided Design and Computer Graphics, p. 6. IEEE (2005)
23. Deb, K.: Multi-Objective Optimization Using Evolutionary Algorithms. Wiley, New York (2001)
24. MATLAB: version 9.6.0.1214997 (R2019a). The MathWorks Inc., Natick, Massachusetts (2019)
25. SIMPLIFY3D, I.S.S.: version 4.0.0 (2017). Simplify3D LLC., Legal Dept, Simplify3D (2017)